On the interplay between symmetry breaking, integrability, and chaos in the semiclassical limit of the Heisenberg system

G. Q. Pellegrino, K. Furuya, and M. C. Nemes

Citation: Chaos **5**, 463 (1995); doi: 10.1063/1.166118

View online: http://dx.doi.org/10.1063/1.166118

View Table of Contents: http://scitation.aip.org/content/aip/journal/chaos/5/2?ver=pdfcov

Published by the AIP Publishing

On the interplay between symmetry breaking, integrability, and chaos in the semiclassical limit of the Heisenberg system

G. Q. Pellegrino and K. Furuya
Instituto de Física "Gleb Wataghin," Universidade Estadual de Campinas, UNICAMP, 13083-970, Campinas, São Paulo, Brazil

M. C. Nemes
Departamento de Física, Instituto de Ciências Exatas, Universidade Federal de Minas Gerais, 31270-901, Belo Horizonte, Minas Gerais, Brazil

(Received 10 January 1994; accepted for publication 7 September 1994)

In this work we present a detailed numerical analysis of the interplay between symmetry breaking, integrability, and chaos in the two- and three-spin Heisenberg models. The results suggest that a very simple and powerful tool to convey such information are the plots of the energy level spacings Δ_n versus the energy level index n, together with the correlation plots $\Delta_{n+1}\times\Delta_n$. When integrability is broken, these plots are shown to identify very sharply an energy below which one has chaotic behavior. The particularly strong point in favor of such analysis is that it can be useful in partially chaotic regimes. © *1995 American Institute of Physics.*

I. INTRODUCTION

Among several systems, models characterized by Heisenberg interactions have been explored through the years in many different contexts. They have proven to be valuable tools either in statistical mechanics to understand magnetic to non-magnetic transition phenomena in lattice spin systems; or in the few degrees of freedom context to study chaotic dynamics;[1] or else to study the consequences of symmetry breaking in the correspondence between quantum energy spectra and classical periodic orbits in the integrable two-spin Heisenberg model.[2]

In this work we present a detailed analysis of the interplay between symmetry breaking, integrability, and chaos in the two- and three-spin Heisenberg models. The study is essentially numerical and shows that important aspects of this interplay can be evidenced in a very conspicuous way by means of the following plots: the energy level spacings Δ_n versus the energy level index n and the correlation graphs $\Delta_{n+1}\times\Delta_n$. We show that in the three-spin case such plots give a very clear signature of the energy range where chaos starts setting in and the one where the corresponding classical dynamics exhibits coexisting regular and irregular orbits; also, we can establish a critical value for the energy above which the classical dynamics is known to have only regular behavior.[1]

A similar study has been performed in Refs. 3–6 for infinite Hilbert space systems, i.e., systems for which the classical limit is attained as the energy level index n tends to infinity. Our case shows remarkable differences. For instance, the finite Hilbert space coming from spin-like degrees of freedom (for finite spin size S) gives us finite spectra. With the large S scaling property, well known for these Heisenberg models,[2] we can scale the whole spectra by $J\hbar^2S(S+1)$. This scaling by $J\hbar^2S(S+1)$ fixes the lower and upper extrema of the spectra at values independent of S (for large S) which means that we can globally explore the entire spectra in the semiclassical limit, without suppressing their low energy part as it is usually done for particle system spectra. By the same token, since the classical limit for these spin systems is attained as S increases, controlling S allows for a control of the approximation to the classical limit for the spectrum as a whole. It also provides a way to investigate and control the density of states in a given region of the spectrum. Thus, the features coming from the finiteness of the Hilbert space and from the well defined classical limit settles a different context, as compared to the particle-system case. In this spin-system situation, it will be shown that the plots originally used by Hirooka *et al.*[3] in a particle-like context can give much (specific and general) information in a form that can be easily connected to basic physical concepts.

To carry out this proposal we studied the two- and three-spin anisotropic Heisenberg models concerning effects that appear in three distinct situations, namely:

(i) effect of symmetry breaking (by varying an anisotropy parameter), without breaking integrability;
(ii) effect of increasing the number of spins, keeping integrability;
(iii) effect of symmetry breaking with concomitant breaking of integrability.

In the two-spin integrable case, symmetry breaking induces a partial folding in the correlation plot $\Delta_{n+1}\times\Delta_n$. In the three-spin integrable case the high degree of degeneracy of the spectrum gives an analogous result once one removes the degeneracy by a well defined procedure: one takes only one level as representative of all the corresponding degenerate ones and uses the so obtained spectrum to study $\Delta_{n+1}\times\Delta_n$. Following this prescription one obtains a figure which is analogous to that obtained for the two-spin isotropic case. Based on this result a similar procedure is used to study cases of small departures from integrability.

Despite the possibility of going into the region of the anisotropy parameter where chaos is most prevalent, we shall see that the most profitable point of these tools resides in the possibility of working in the transition region between very weakly chaotic and moderately chaotic regimes. Namely, they can be useful to get some guiding information on where

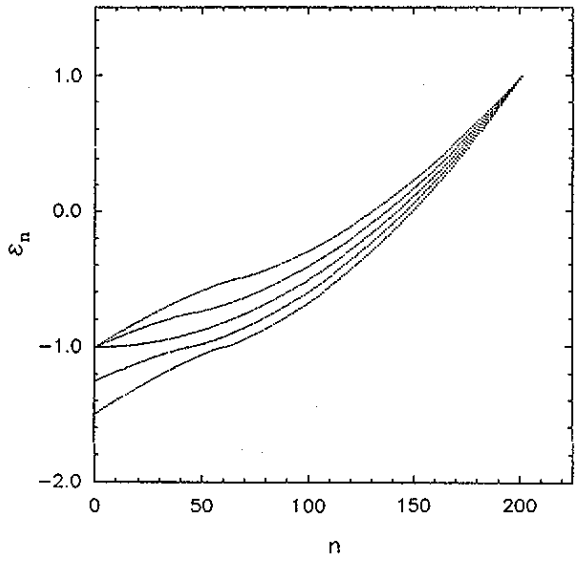

FIG. 1. Spectral distributions of the two-spin system for spin size $S=200$ and some values of the anisotropy parameter: $\sigma=-0.5,-0.25,0.0,0.25,0.5$. The lowest spectra correspond to the greatest values of σ.

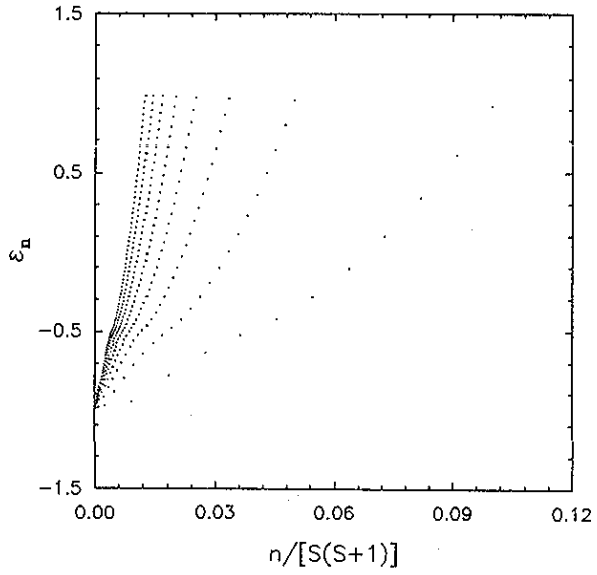

FIG. 2. Spectral distributions of the two-spin system for a single value of the anisotropy parameter, $\sigma=-0.5$, and several values of the spin size, $S=10,20,30,\ldots,80$. Notice how the spectral distribution attains a limiting curve as S increases.

to apply more sophisticated techniques in searching for quantum manifestations of chaos. Also, they can be easily applicable in cases where it is not so simple to separate the symmetries in order to apply techniques based on Random Matrix Theory.[7]

The remainder of this article is organized as follows. In Sec. II we introduce general features of the two- and three-spin systems. In Sec. III we review and analyze the two-spin model, presenting some known results and the plots $\Delta_{n+1}\times\Delta_n$ and $\Delta_n\times n$ obtained for it. In Sec. IV the same procedure is followed for the three-spin model, along with the appropriate comparisons with the guiding integrable two-spin model of Sec. III. To facilitate the presentation and the understanding of the role played by the symmetry breaking, both sections are divided into three parts: a brief review of the model in question, the isotropic case and the anisotropic one. A last section is devoted to discussions and concluding remarks. Finally in Appendix A we deal with the approximation to the classical limit and in Appendix B we study some wavefunctions of the nearly integrable three-spin case to give support to the procedure taken in the plots for this same case.

II. THE MODELS: TWO-SPIN AND THREE-SPIN SYSTEMS

In this work we deal with two- and three-spin models represented by Hamiltonians

$$H_2=J(\mathbf{S}_1\cdot\mathbf{S}_2+\sigma S_1^z S_2^z) \tag{1}$$

and

$$H_3=J\sum_{i=1}^{3}(\mathbf{S}_i\cdot\mathbf{S}_{i+1}+\sigma S_i^z S_{i+1}^z), \tag{2}$$

where $\mathbf{S}_4\equiv\mathbf{S}_1$, J and the anisotropy parameter σ are real numbers, and S_i^x, S_i^y, S_i^z $(i=1,2,3)$ correspond to the usual $SU(2)$ spin operators. Special attention is paid to the transition from the isotropic case ($\sigma=0$) to the anisotropic one ($\sigma\neq 0$), carried through the variation of the symmetry breaking parameter σ. Throughout this work we set $\hbar=1$ and $|\mathbf{S}_i|=S$ $(i=1,2,3)$.

Some general features to be noticed are the following:

(i) The Hilbert spaces associated with systems (1) and (2) are finite. This feature comes from the $SU(2)$ Lie algebra of spin operators and guarantees that the energy spectrum is itself finite.

(ii) Systems (1) and (2) have well defined classical limits. As stressed in Ref. 2, these Heisenberg models belong to a class named Curie-Weiss models and are characterized by a large S scaling behavior. This scaling property guarantees the existence of their classical limits, which can be shown to be unique for these Heisenberg models.[8]

(iii) The isotropy breaking has important effects on the integrability of the models. While the two-spin system is integrable for all values of σ,[2] the three-spin system is shown by Nakamura and Bishop[1] to be integrable for $\sigma=0$ and non-integrable for $\sigma\neq 0$ (and $S>1/2$). This last case presents associated classical phase space and energy spectra possessing, both, regions of regular motion associated with periodic orbits, and regions of irregular motion associated by the authors to chaos followed by destruction of KAM tori.

III. TWO-SPIN MODEL

A. Brief review of the model

The integrable anisotropic Heisenberg two-spin model is given by Hamiltonian (1):

$$H_2 = J(\mathbf{S}_1 \cdot \mathbf{S}_2 + \sigma S_1^z S_2^z).$$

From the equation above it is easily seen that, besides the energy, this model has the z-component T_2^z of the total spin

$$\mathbf{T}_2 = \mathbf{S}_1 + \mathbf{S}_2 \tag{3}$$

as a constant of motion:

$$[H_2, T_2^z] = 0. \tag{4}$$

Since we have set $|\mathbf{S}_1| = |\mathbf{S}_2| = S$, we diagonalize H_2 using as basis states the tensor product of spin states, defined as

$$|m_1 m_2\rangle \equiv \frac{1}{2!}[|S,m_1;S,m_2\rangle \pm |S,m_2;S,m_1\rangle], \tag{5}$$

where the $+(-)$ sign corresponds to bosonic (fermionic) states. Throughout this section we work within the subspace where $\langle T_2^z \rangle = 0$ which implies the relation $m_1 + m_2 = 0$ for m_1 and m_2, the quantum numbers corresponding to the z-projection of the spin operators $\mathbf{S}_1$ and $\mathbf{S}_2$, respectively. Also, we restrict ourselves to the antiferromagnetic case $J > 0$, with $J = 1$ (Ref. 9) and integer values for S, meaning that we deal here with the bosonic case [+ sign in Eq. (5)].[10]

Figure 1 shows typical spectra for the spin size $S = 200$ (sufficiently large to illustrate the results) and some values of the anisotropy parameter σ.

The large S scaling behavior can be observed in Fig. 2: as the spin size tends to infinity, the quantum spectrum tends to its classical limit in the form of a universal curve. We remark here that, for this model, the spectra are all nondegenerate. As we can see, in all these figures the energy is scaled by $J\hbar^2 S(S+1)$. This scaling tends to fix the endpoints of the finite scaled spectrum at values that, in the classical limit, do not depend on S, depending only on σ. From Fig. 2 it can easily be seen that, for a given value of σ, the number of energy levels increases with S, diminishing in this way the energy difference between two neighboring levels, the scaled energy range being now fixed. This allows the control of the approximation to the classical limit by changing the value of S. Details of this aspect are given in Appendix A.

B. Isotropic case ($\sigma = 0$)

Figures 3(a)–3(c) show altogether the two-spin isotropic case ($\sigma = 0$) for $S = 200$. The spectrum is shown in Fig. 3(a) and in Figs. 3(b) and 3(c) we plot respectively $\Delta_{n+1} \times \Delta_n$ and $\Delta_n \times n$ where, in general,

$$\Delta_n = \epsilon_{n+1} - \epsilon_n \tag{6}$$

is the (scaled) energy difference between the $(n+1)$-th and the n-th levels. These figures show typical quantum rotor spectra. Moreover, they are useful to establish concepts and vocabulary which will appear in the next sections.

One of the points to explore is to see numerically how the classical limit of the spectrum is approximated. The analysis using the data of Fig. 3(a) is given in Appendix A, and shows that for $S = 200$ one is essentially working with $\hbar \approx 5 \times 10^{-3}$. Once we have made sure that we are in a regime which can be considered nearly classical, let us present some useful associations concerning the plots. For example, the plot of Fig. 3(c) reflects the density of states ρ per energy unity

$$\rho = \frac{1}{d\epsilon/dn}, \tag{7}$$

which is higher at lower energy values. In a sense we can say that the region around the minimum in Fig. 3(a), with $\epsilon = -1.0$, meets semiclassical characteristics "faster" than other regions, a feature that can be used to indicate where we can safely apply the semiclassical methods much in use to study chaos and other classical structures.[11] In similar ways, this behavior seems to be common to other integrable systems with finite Hilbert space, like the $SU(2)$ Lipkin model.[12]

In Ref. 2 advantage was taken of the existence of the classical limit to link the quantum spectra to the classical actions of periodic orbits, obtained for this model via the use of coherent states. Here we present a simple argument after which this link can be made straightforward with the use of the plot $\Delta_n \times n$. In Fig. 3(c) the step length in the variable n is $dn = 1$. Thus we have plotted in fact

$$\epsilon_{n+1} - \epsilon_n = \frac{\epsilon_{n+dn} - \epsilon_n}{dn}. \tag{8}$$

In the classical limit this is simply $d\epsilon/dn$ and n is, apart from scale factors, the action $\mathscr{S}$ of the periodic orbit with energy ϵ. Thus we have in Fig. 3(c)

$$\frac{\epsilon_{n+dn} - \epsilon_n}{dn} \approx A \frac{d\epsilon}{d\mathscr{S}} = A\nu, \tag{9}$$

the (scaled) frequency ν of the corresponding periodic orbit (the constant A stands for the scale factors). It can be seen in Fig. 3(c) that, as a result of the finiteness of the associated Hilbert space and of the integrability of this case, the plot $\Delta_n \times n$ reveals a finite range of well defined frequencies for the periodic orbits.[13]

As a final remark concerning isotropy, we observe that a characteristic that comes immediately into sight is the single line showed by Fig. 3(b). This is reflected in Fig. 3(c) as a one-to-one correspondence: to each allowed frequency is associated a unique energy, or a unique periodic orbit.

C. Anisotropic case ($\sigma \neq 0$)

The two-spin anisotropic case is represented in the set of Figs. 4(a)–4(c) with the illustrative values $\sigma = -0.5$ and $S = 200$. Notice that the isotropy breaking changes the spectral curve, there appearing an inflection point at energy $\epsilon_{ip} = -1.0 + |\sigma|$ for $-1.0 \leqslant \sigma \leqslant 0.0$ [see Fig. 4(a)]. Furthermore the point of the spectrum with highest density of levels, shown as an inverted peak in Fig. 4(c), accompanies this inflection point. The discussion on the classical limit is still valid and Fig. 4(b) shows that there is a correlation between Δ_{n+1} and Δ_n in this case also. Although not so simple a correlation as in the $\sigma = 0$ case, one can argue (see Appendix A) that here again we are in a safe ground concerning classical approximation, and the isotropic case can be used to calibrate such approximation.

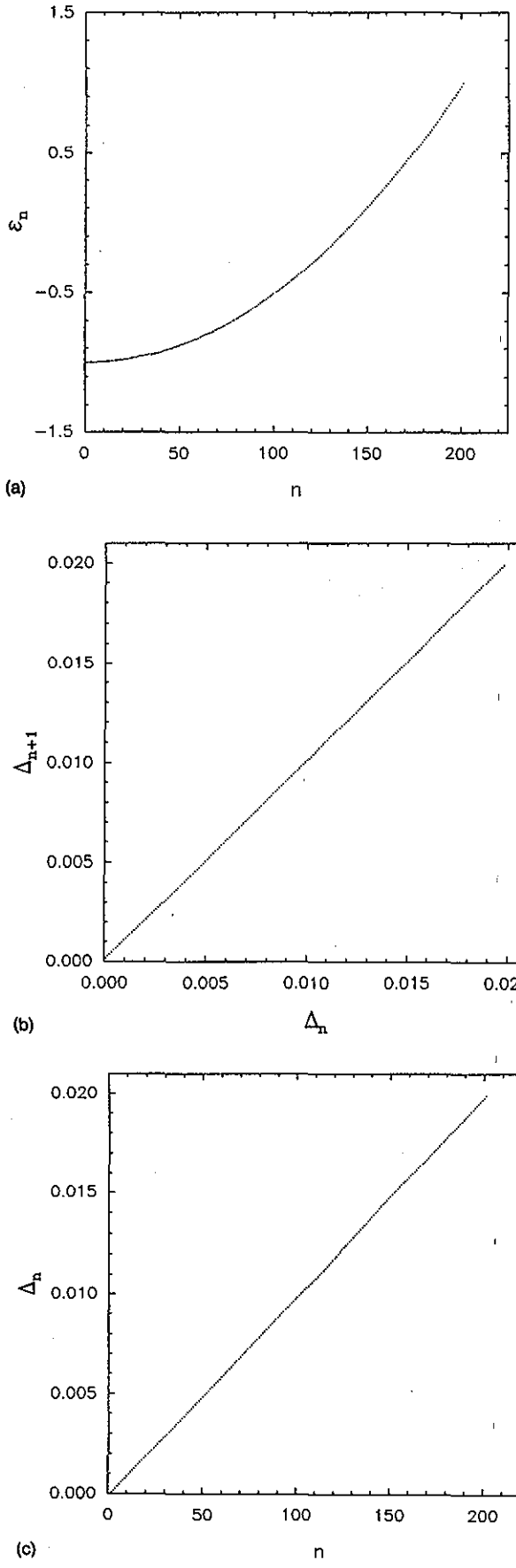

FIG. 3. The two-spin isotropic case ($S=200$ and $\sigma=0.0$): (a) spectral distribution; (b) energy difference correlation plot $\Delta_{n+1}\times\Delta_n$; (c) energy level difference Δ_n versus the energy level index n.

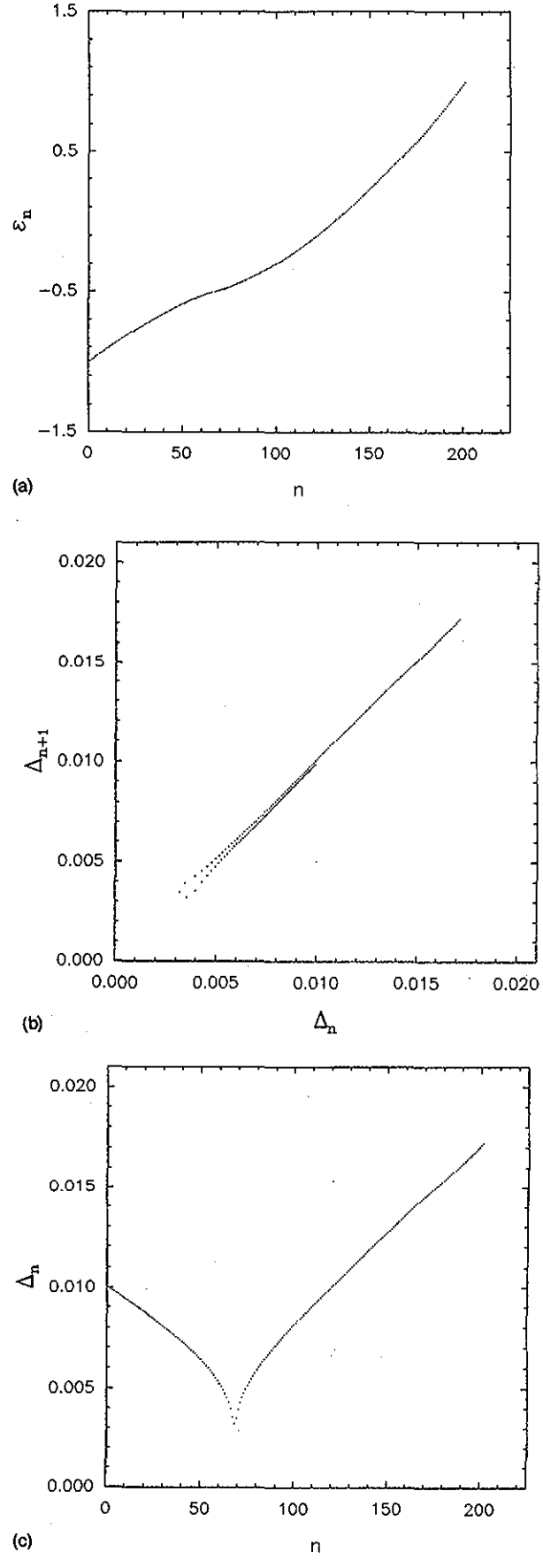

FIG. 4. The same as in Fig. 3. Here it is shown the two-spin anisotropic case ($S=200$ and $\sigma=-0.5$).

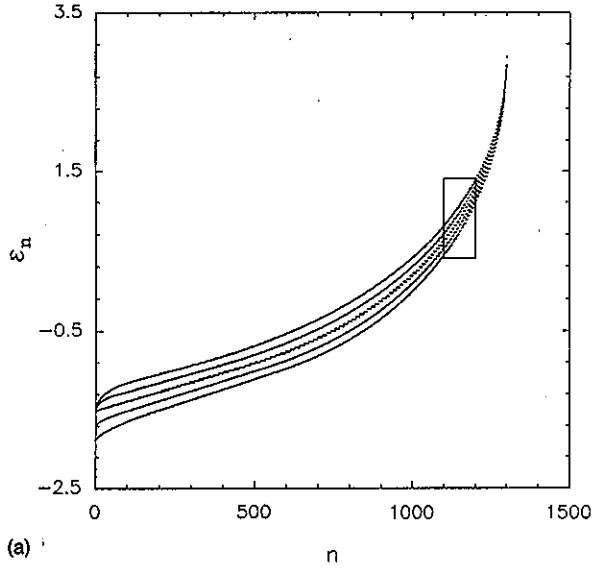

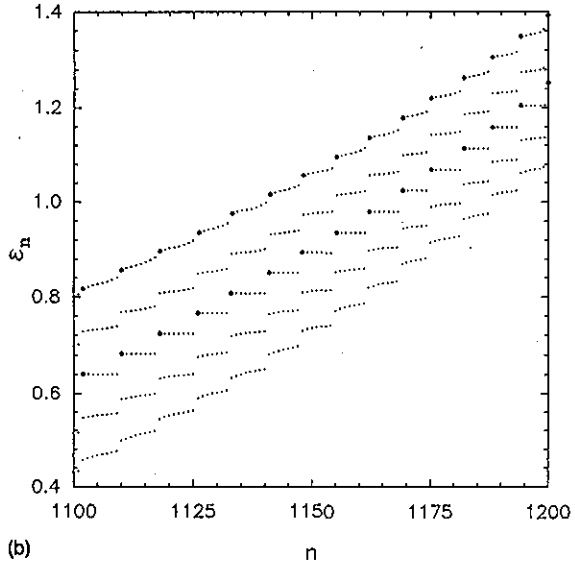

FIG. 5. (a) Spectral distributions of the three-spin system for spin size $S=50$ and some values of the anisotropy parameter: $\sigma=-0.5,-0.25,0.0,0.25,0.5$. The lowest spectra correspond to the greatest values of σ; (b) blow up of the squared region in (a), where the solid circles exemplify the procedure of picking up appropriate spectra for two cases: $\sigma=0.0$ and $\sigma=-0.5$ (upper points).

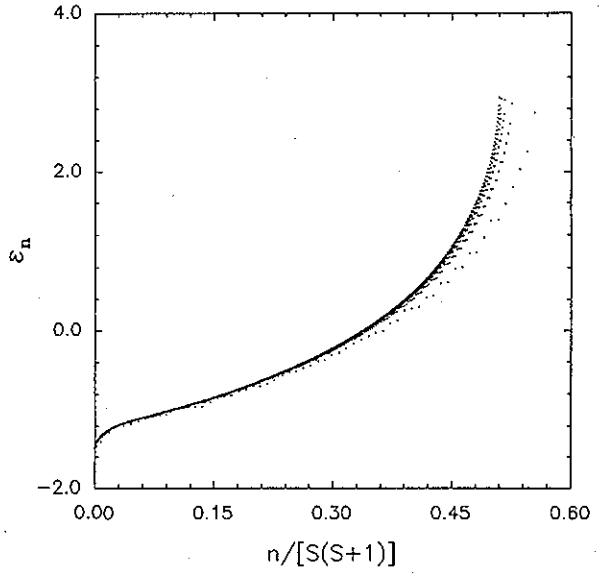

FIG. 6. Spectral distributions of the three-spin system for a single value of the anisotropy parameter, $\sigma=-0.5$, and several values of the spin size, $S=10,20,30,40,50$. Notice how the spectral distribution attains a limiting one as S increases.

Figure 4(c) displays, as in the previous subsection, a finite range of frequencies with a special point where the frequency tends to zero as the classical limit is attained. Since this inverted peak corresponds to the inflection point in the spectrum, we can be sure of the existence of a periodic orbit—for the system is integrable—with an infinite period. This is in complete agreement with the results presented in Ref. 2 where the inflection point in the spectrum is shown to correspond to a separatrix orbit with analytically calculated infinite period. Besides, as can be seen in Fig. 4(c), this inflection point is in the center of the region of highest level density. It can be shown that the density of levels ρ has its maximum variation with increasing S at the inflection point, i.e., $d\rho/dS$ has a (positive) maximum at the inflection point. We therefore expect stronger manifestations of chaotic behavior (in the non-integrable case) to occur in this region. In Ref. 14 one can learn that the two-spin model can become chaotic after the introduction of local anisotropies. In this way Fig. 4(c) suggests that the region around the inflection point, i.e., around the separatrix orbit, would be the appropriate region where to look for manifestations of classical chaotic dynamics. This suggestion agrees with our expectation that, as chaos sets in, it is in the separatrix region that irregular orbits start appearing.

Concerning the isotropy breaking, we see in Fig. 4(b) that the straight line of the isotropic case [see Fig. 3(b)] presents a folding. Notice that the lower string in Fig. 4(b) corresponds to the one at the left side of the inverted peak in Fig. 4(c). We can also see in Fig. 4(c) that in this anisotropic case the one-to-one correspondence between frequencies and energies is broken: in the region around the vanishing frequency there exists two different energies, i.e., two different periodic orbits, with the same period.

IV. THREE-SPIN MODEL

A. Brief review of the model

The anisotropic Heisenberg three-spin model is given by Hamiltonian (2),

$$H_3=J\sum_{i=1}^{3}(\mathbf{S}_i\cdot\mathbf{S}_{i+1}+\sigma S_i^z S_{i+1}^z),$$

where $\mathbf{S}_4\equiv\mathbf{S}_1$. We will concentrate on the antiferromagnetic interaction $J>0$, fix $J=1$ and choose equal all the spin values, $|\mathbf{S}_i|=S$ $(i=1,2,3)$.

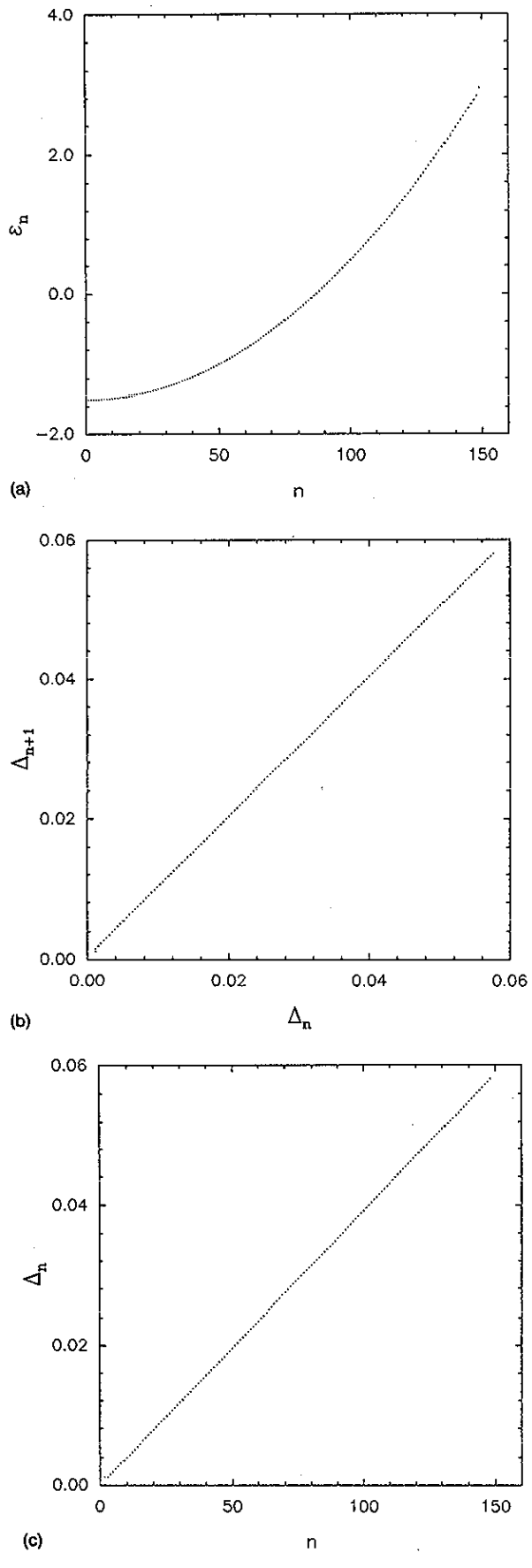

FIG. 7. The three-spin isotropic case ($S=50$ and $\sigma=0.0$): (a) spectral distribution selected according to the procedure shown in Fig. 5(b) ; (b) energy difference correlation plot $\Delta_{n+1}\times\Delta_n$; (c) energy level difference Δ_n versus the energy level index n.

As in the previous two-spin case, this model has as a constant of motion the z-component T_3^z of the total spin:

$$\mathbf{T}_3=\mathbf{S}_1+\mathbf{S}_2+\mathbf{S}_3, \tag{10}$$

since

$$[H_3,T_3^z]=0, \tag{11}$$

and we will be working within the subspace where $\langle T_3^z\rangle=0$. For future reference we note that the operator $\mathbf{T}_3^2$ is also a constant of motion for the isotropic case $\sigma=0$. Since each $\mathbf{S}_i^2$ is individually a constant, the expression for $\mathbf{T}_3^2$ resulting from Eq. (10) is

$$\mathbf{T}_3^2=3S(S+1)+2\sum_{i=1}^{3}\mathbf{S}_i\cdot\mathbf{S}_{i+1}. \tag{12}$$

Notice that the second term on the right-hand side of Eq. (12) is just the Hamiltonian H_3 with $\sigma=0$ (and $J=1/2$).

The diagonalization of H_3 has been done using the (anti)symmetrized spin states for S (half) integer:

$$\begin{aligned}|m_1m_2m_3\rangle\equiv\frac{1}{3!}\{&|S,m_1;S,m_2;S,m_3\rangle+|S,m_3;S,m_1;S,m_2\rangle\\&+|S,m_2;S,m_3;S,m_1\rangle\pm[|S,m_3;S,m_2;S,m_1\rangle\\&+|S,m_1;S,m_3;S,m_2\rangle+|S,m_2;S,m_1;S,m_3\rangle]\}.\end{aligned} \tag{13}$$

Here, once more, the $+(-)$ sign corresponds to bosonic (fermionic) case, and we restrict ourselves to integer values for S [$+$ sign in Eq. (13)],[10] while $m_1+m_2+m_3=0$ leading to $\langle T_3^z\rangle=0$.

Typical finite spectra for the three-spin model [Eq. (2)] are shown in Fig. 5(a) for $S=50$ and some illustrative values of the anisotropy parameter σ. The squared region of the entire spectra is blown up in Fig. 5(b). From these figures we can see that the spectrum of the isotropic case is highly degenerate, therefore exhibiting a staircase shape. This is due to the many possible ways of constructing the same value of $\mathbf{T}_3^2$ combining three spins, with $\langle T_3^z\rangle=0$. As we slowly turn the anisotropy parameter σ on, the steps of the isotropic spectrum become adiabatically distorted [see Fig. 5(b)]. Moreover, for a given value of σ, this departure from the degeneracy is more pronounced in the lower parts of the anisotropic spectrum, whereas in its upper parts it seems to remain closer to the shape of the isotropic ($\sigma=0$) case. This transition occurs smoothly, so that no sharp values of energy seems to exist to clearly mark such a change of character along the spectrum.

Figure 6 shows the large-S scaling behavior for this three-spin system. This behavior is similar to the one observed in Fig. 2 for the two-spin system, except for the fact that here we have degenerate or nearly degenerate spectra. Though this fact prevents us from speaking of a universal limiting *curve*, there exist a universal limiting spectrum. Apart from this detail, the whole analysis of Fig. 2 can be transported to Fig. 6. It is interesting to notice that the spectra obtained for the anisotropic cases (e.g., $\sigma=-0.5$) show

clearly two regions of distinct curvatures resembling a presence of inflection point as in the integrable two-spin spectra.

On the other hand, degeneracies and near-degeneracies do make considerable differences in the plots $\Delta_{n+1}\times\Delta_n$ and $\Delta_n\times n$. Degenerate levels yield points at the $\Delta_n=0$ axis for the isotropic case ($\sigma=0$), and it is not appropriate to consider them if we want to compare with the plots obtained for the two-spin system (non-degenerate). In order for the comparison to make sense, the most natural and simple thing to do is to eliminate the degeneracies just by counting as one level all the degenerate ones. [Since, as shown by Eq. (12), to each step there corresponds one value of $\mathbf{T}_3^2$, this means taking the spectra mod$\mathbf{T}_3^2$.] It is important to stress the fact that here, in contrast to the two-spin system, we are considering n just as a counting index without any physical interpretation. This procedure gives us a hint of the possible strategy to be followed when we depart slightly from the $\sigma=0$ case: *namely, for the anisotropic spectra we pick up those points* corresponding to the first in each stair step of the isotropic ($\sigma=0$) spectrum. Such a procedure is illustrated in Fig. 5(b), by counting only the energies marked with solid circles. The resulting spectrum contains only one level representative of the nearly conserved quantity $\mathbf{T}_3^2$.[15]

For small values of $|\sigma|$, the overall behavior does not change if we change our criteria and pick up the second point (or the middle point) in the deformed stair steps instead of the first ones. This reflects the fact shown in Appendix B that the eigenstate corresponding to each point of a deformed stair step has a dominant component in one of the states of the corresponding isotropic stair step.[16] As we further increase the value of σ, it does make difference which sequence of points we are choosing for the plots. This is not surprising since the deformation of the stair steps becomes large for larger values of σ; and this is also expected to be so, since one can no longer speak of a dominant value of $\mathbf{T}_3^2$ in the expansion of the anisotropic eigenstate in the basis states of the integrable isotropic case.

In the following subsections we give the details of the above mentioned plots: in Sec. IV B we compare the two- *and three-spin isotropic systems, both integrable cases; and* in Sec. IV C we discuss the effect of breaking isotropy and integrability concomitantly for the three-spin system.

B. Isotropic case ($\sigma=0$)

A selected spectrum and corresponding plots $\Delta_{n+1}\times\Delta_n$ *and* $\Delta_n\times n$ *for the three-spin isotropic case* ($\sigma=0$) for $S=50$ are shown in Figs. 7(a)–7(c). Comparing them with the set of Figs. 3(a)–3(c) of the two-spin system, one can see that both sets are completely analogous, either in the parabolic shape of $\epsilon_n\times n$ or in the plots $\Delta_{n+1}\times\Delta_n$ and $\Delta_n\times n$. This result is not at all obvious, for, if we think in terms of classical phase spaces, we are adding two more dimensions and more constraints. But such a surprising analogy allows us to extend the discussion about the classical limit and the relations implied on the value of $\hbar$ (see the end of Appendix A).

From a broader point of view we note that the isotropic two- and three-spin models are one degree of freedom systems, possessing both of them classical integrable analogues.[2,1] The integrability of this $\sigma=0$ case is reflected in Fig. 7(c). This typically smooth behavior, simultaneously with the regularity implied by relations (A3) and (A4), reflects the existence of only periodic orbits for this case, that is, for $\sigma=0$ the system is integrable. In this sense our analysis of the regularly spaced (selected) energy levels, seen in Fig. 7(c), agrees with the analysis of this integrable case presented by Nakamura and Bishop in Ref. 1, where the regular stair steps of clustered levels are seen as quantum counterparts of classical periodic orbits.

C. Anisotropic case ($\sigma\neq0$)

As mentioned before, Ref. 1 shows that the isotropy breaking produces also the breaking of integrability for the three-spin system (breaking the constant of motion $\mathbf{T}_3^2$). The corresponding classical analogues exhibit coexisting regular and irregular orbits in a regime depending on the absolute value of σ: the greater is $|\sigma|$, the more chaotic is the regime.

Figures 8(a)–8(c), 9(a)–9(c), and 10(a)–10(c) show the plots for selected spectra picked up from the full ones, obtained for $S=50$ and $\sigma=-0.05$, -0.1, -0.3, respectively. The already explained procedure of picking up levels from *the deformed stair steps is what allows for a comparison with* the corresponding figures of the anisotropic two-spin model (no comparison would be possible without our picked up spectra). To begin with, we assure that also here we do have a good control of the approximation to the classical limit since, for each value of σ, the spectrum of the isotropic case can be regarded as a gauge. The second point to be noticed is that it can be seen from Figs. 8–10 that the spectra for $\sigma\neq0$ have critical values of level index, n_c, above which they show regular and correlated sequential energy differences Δ_n. This critical value n_c is a function of σ, increasing with increasing $|\sigma|$. In Sec. IV A we advanced this tendency of the full spectrum to recover the staircase shape of the integrable $\sigma=0$ case, noting however that there it could be difficult to point out a definite value for the energy at which this would happen. These plots $\Delta_n\times n$ give us, instead, a precise value for n_c and a corresponding value for a critical energy ϵ_c above which we can state the regularity of the spectrum. This analysis agrees with the analysis of the quantum spectra presented by Nakamura and Bishop,[1] their indicative values for ϵ_c lying slightly below those provided by the plots $\Delta_n\times n$.

In the integrable two-spin model the breaking of anisotropy was associated with the appearance of an inflection point in the corresponding spectrum, marking the presence of a separatrix orbit in its classical analog. In the plots $\Delta_n\times n$ this inflection point is translated as an inverted peak denoting both an infinite period for the separatrix orbit and a region of high density of states. We then argued that this region should be the appropriate region to look for manifestations of chaos in a chaotic version of the model. These ideas can be pursued also here. First we notice that, as we go farther from $\sigma=0$, the spectra in Figs. 8(a)–10(a) acquire two distinctive curvatures as if they had an inflection point with a behavior similar to the one observed in Fig. 4(a). Of course this is not a true inflection point since the spectra are not smooth curves, as

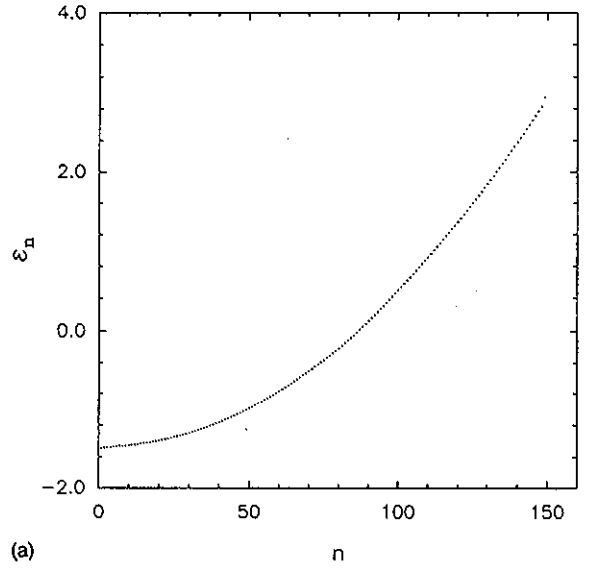

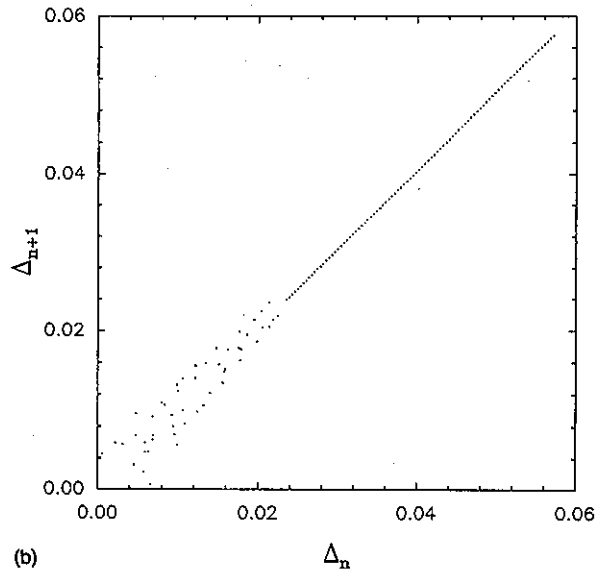

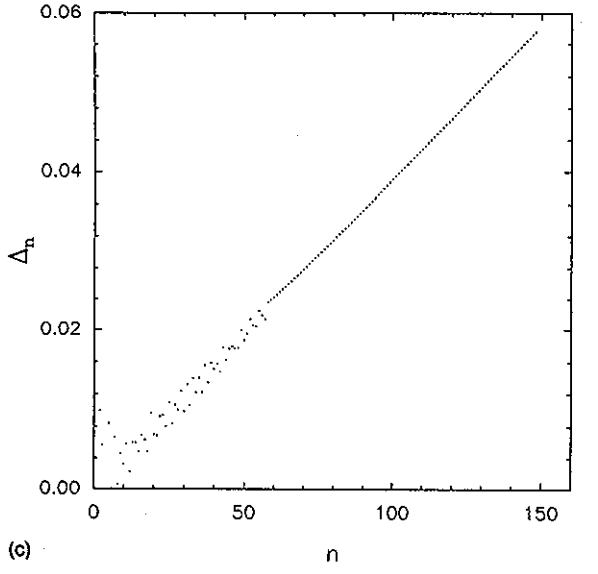

FIG. 8. The same as in Fig. 7. Here it is shown the three-spin anisotropic case ($S=50$ and $\sigma=-0.05$).

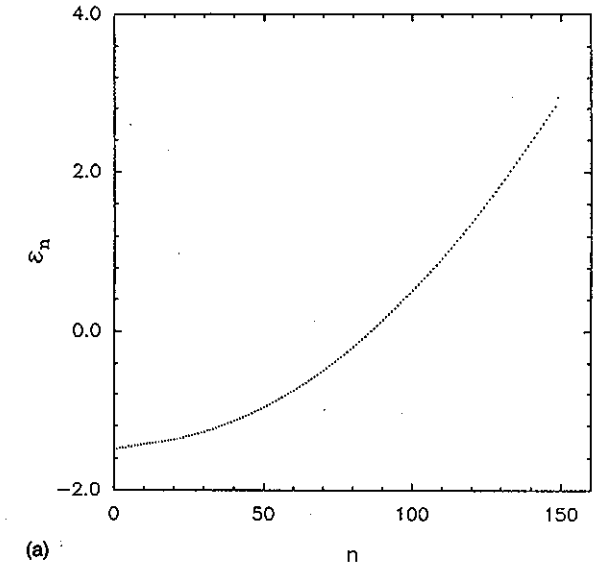

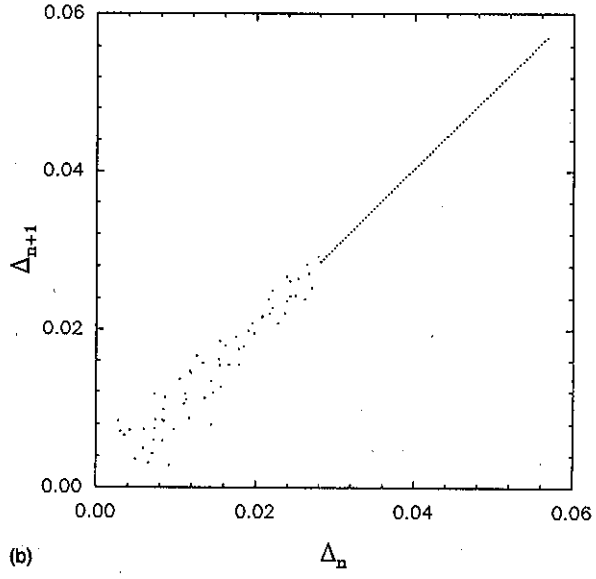

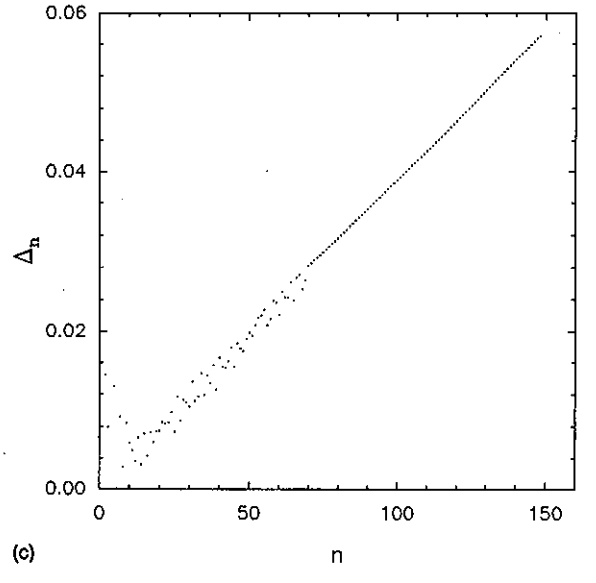

FIG. 9. The same as in Fig. 7. Here it is shown the three-spin anisotropic case ($S=50$ and $\sigma=-0.1$).

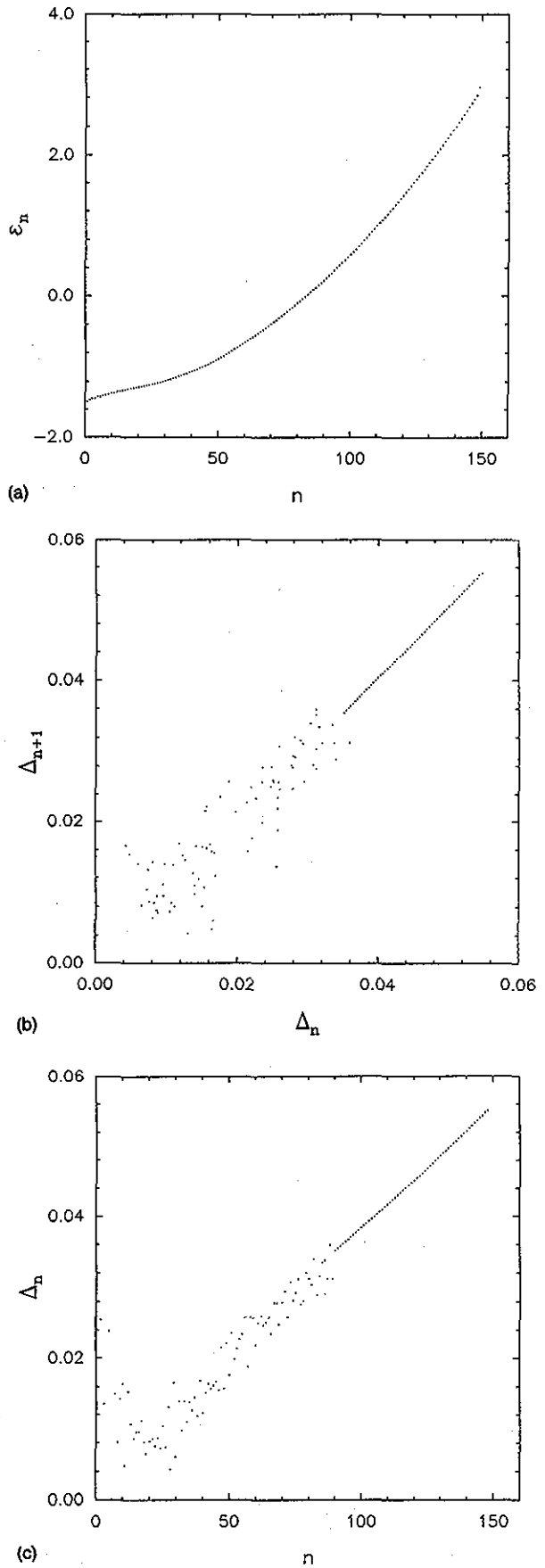

FIG. 10. The same as in Fig. 7. Here it is shown the three-spin anisotropic case ($S=50$ and $\sigma=-0.3$).

we can see in Figs. 8(c)–10(c). Even so, the global behavior of the points in Figs. 8(c)–10(c) suggests the presence of an inverted peak accompanying this pseudo-inflection point in the spectrum [compare with Fig. 4(c)]. Analogously to what we did with the two-spin model, here we believe that the region around this inverted peak is the good region to see where chaos starts setting in as $|\sigma|$ increases. In fact, the Poincaré sections of Ref. 1 indeed corroborates this idea, showing some of the most chaotic sections around the energy of the pseudo-inflection point.

Figures 8(c)–10(c) suggest the following values of level indices n_{ip} and corresponding energies ϵ_{ip} for the inverted peaks, according to the value of σ:

(a) for $\sigma=-0.05$, $n_{ip}\approx 10$ with $\epsilon_{ip}\approx -1.45$;
(b) for $\sigma=-0.1$, $n_{ip}\approx 12$ with $\epsilon_{ip}\approx -1.42$;
(c) for $\sigma=-0.3$, $n_{ip}\approx 22$ with $\epsilon_{ip}\approx -1.26$.

The regions of the corresponding spectra around these values represent the energy range where chaos is more easily observed. As we go farther away from these regions, regular orbits are more and more likely to coexist with the irregular ones, until those become predominant. As we cross the critical energy ϵ_c, we enter the completely regular part of the spectrum where only regular orbits can be observed. We remark that this inflection-point approach agrees with the analysis proposed by Nakamura and Bishop[1] using second order differences of the energy with respect to σ. In special we note that the regions around the values presented in items (a), (b), and (c) lie inside the chaotic regions presented in Ref. 1, not excluding the possibility that, for greater values of σ, regular orbits can be observed even at low energies near the ground state.

We finish this section with a few remarks concerning the transition isotropy $\rightarrow$ anisotropy. Figures 8(b)–10(b) show points lying in a planar region of the coordinate system $\Delta_{n+1}\times\Delta_n$. It is suggestive that the anisotropy already caused a folding below certain $n_c(\sigma)$ in the line appearing in the integrable two-spin plots $\Delta_{n+1}\times\Delta_n$. In these three-spin cases we seem to have a combination of folding and "mixing" of the points below the corresponding $n_c(\sigma)$. This surprising behavior calls one's attention to its similarity with the behavior presented by other sets of points that appear in the studies related to fractal dimension.[17] Interesting in its own right, this suggestion is presently being investigated.

V. DISCUSSION AND CONCLUSIONS

In the present contribution we studied several cases of spin models, making use of simple energy difference plots $\Delta_{n+1}\times\Delta_n$ and $\Delta_n\times n$. In special we showed that much information can be obtained from these plots concerning the transitions isotropy $\leftrightarrow$ anisotropy and integrability $\leftrightarrow$ nonintegrability, together with the breaking of a constant of motion. More specifically we studied these transitions in the cases:

(i) isotropy breaking keeping integrability for the two-spin model, where we confirmed the presence of an inflection point in the spectrum, associated with a separatrix orbit;

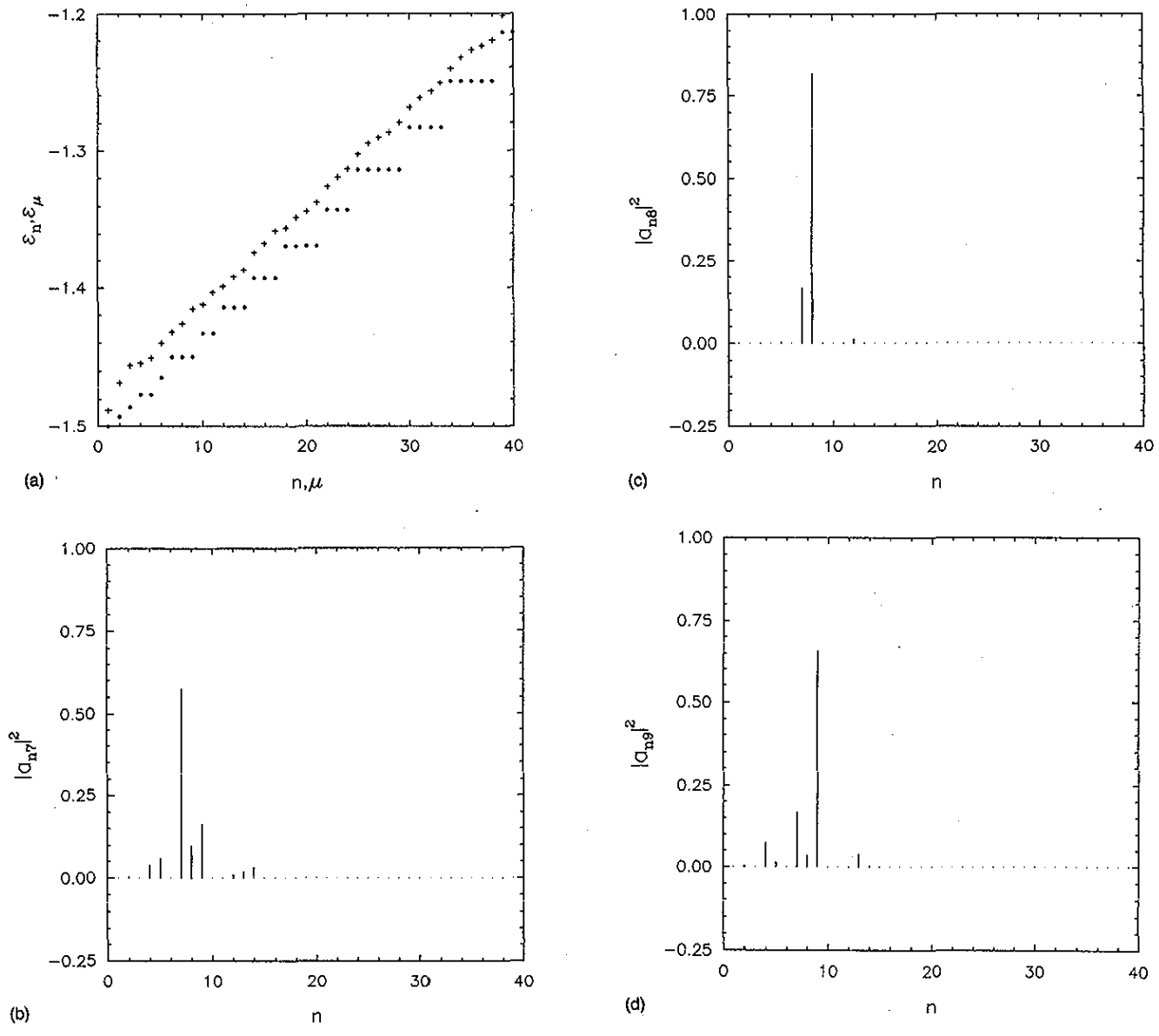

FIG. 11. (a) Blow-up of the region of the spectra for $\sigma=0.0$ (solid circles) and $\sigma=-0.05$ (crosses) from where the states $|\psi_\mu\rangle$ are chosen [the horizontal axis refers identically to both indices μ and n and the vertical axis refers to the energy levels ϵ_μ (crosses) and ϵ_n (solid circles)]; (b) projection coefficients $|a_{n\mu}|^2$ versus the isotropic energy level index n for $\mu=7$; (c) the same as in (b) for $\mu=8$; (d) the same as in (b) for $\mu=9$.

(ii) increasing of the number of spins keeping integrability, where we showed that the plots used allow one to compare, on the basis of simple concepts, such distinct systems as those obtained in going from two to three spins;

(iii) isotropy breaking with concomitant breaking of integrability for the three-spin model, where surprisingly the nearly integrable behavior of the two-degree-of-freedom system can be understood in terms of the integrable one-degree-of-freedom two-spin system.

In addition we have shown that, in general, the plots used provide a way to control the approximation to the classical limit in these systems, a procedure that can be very useful in numerical calculations. Also, the information so obtained could be translated in terms of basic physical concepts such as separatrix, the derivative of the energy with respect to the action and so on.

The fluctuation properties of spectra of systems with coexisting integrable and non-integrable behavior is not yet completely understood in the context of Random Matrix Theory.[18] In such a mixed, non-ergodic regime, the plots we use in the present paper may be helpful in the sense that they can give guiding clues in the study of these regimes. We emphasize herein that these plots are not intended to have the same status of the above mentioned theory; in fact, they are not really comparable. To make this distinction clear, two points are in order. First, Random Matrix Theory, based on rigorous mathematical grounds, provides a detailed and

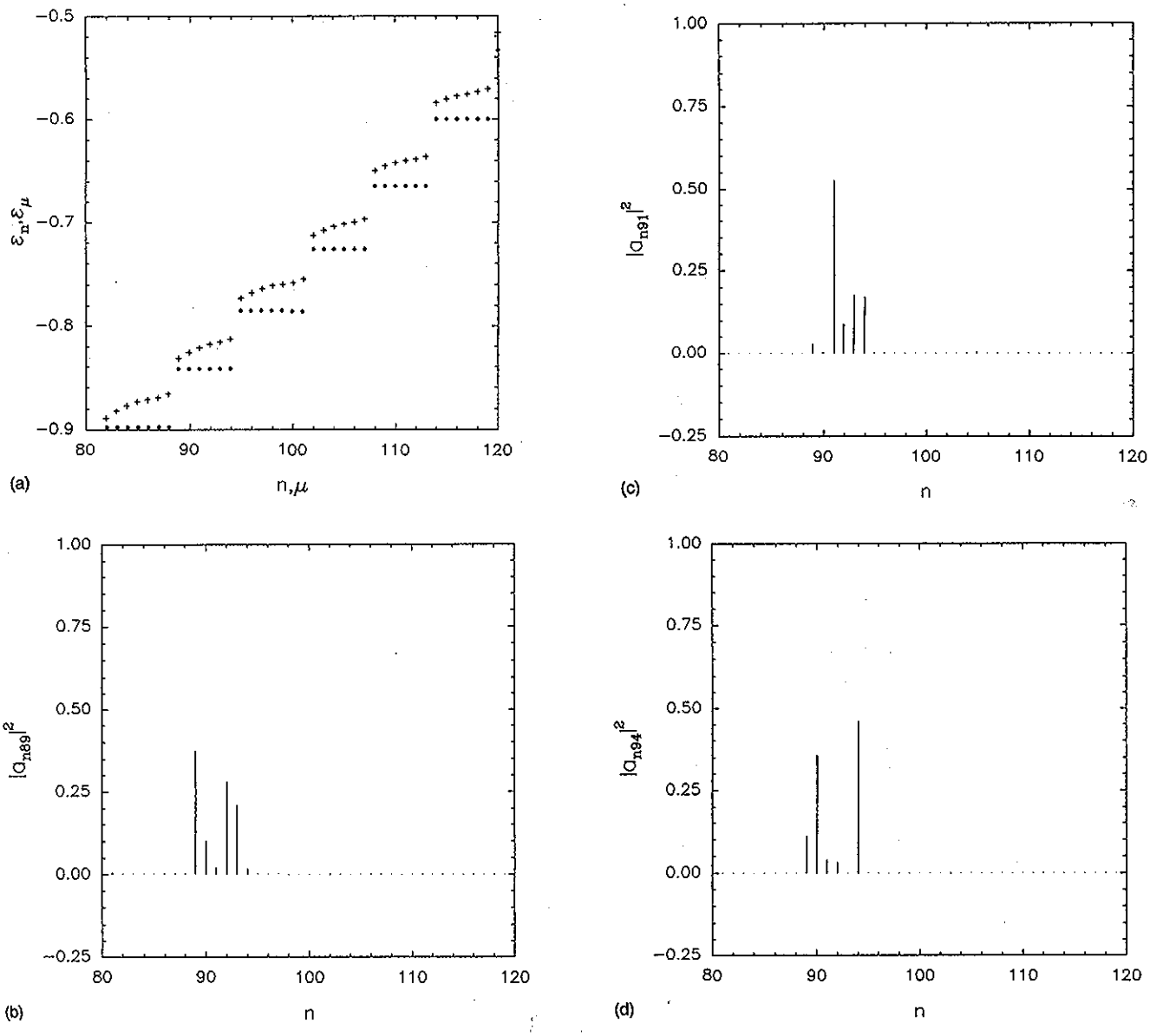

FIG. 12. (a) The same as in Fig. 11(a); (b) the same as in Fig. 11(b) for $\mu=89$; (c) the same as in (b) for $\mu=91$; (d) the same as in (b) for $\mu=94$.

quantitative description of the properties of chaotic system spectra; while the plots here used provide an indicative and qualitative analysis of energy regions where chaos manifests itself. Second, Random Matrix Theory to be applied asks for a complete knowledge of the symmetries involved and also of how to separate them, which can be a difficult task. The main practical advantage of the plots we present resides, instead, in their simple construction and ready applicability. Thus, Random Matrix Theory and our analysis act on different domains and at different informational levels, providing, nevertheless, information which can be complementary and helpful to one another. This discussion was shown to be particularly justified in the perturbative regime of small departures (small $|\sigma|$) from the isotropic case in the three-spin model (supported by the wavefunction analysis presented in Appendix B). But the plots can also be surprisingly meaningful for larger values of $|\sigma|$, which means much stronger chaotic regimes. More detailed wavefunction analysis for these last regimes is under investigation.

Although in this paper we studied the particular case of the Heisenberg models, we believe the procedure to be quite general and useful in the study of other spin systems and in special to other Curie-Weiss systems such as the Lipkin model[19] and the Pairing model.[20] Work along these lines is in progress.

ACKNOWLEDGMENTS

It is a pleasure to acknowledge M. Saraceno and A. F. R. de Toledo Piza for helpful and illuminating discussions. This work was partially supported by FAPESP (Brazil). G.Q.P.

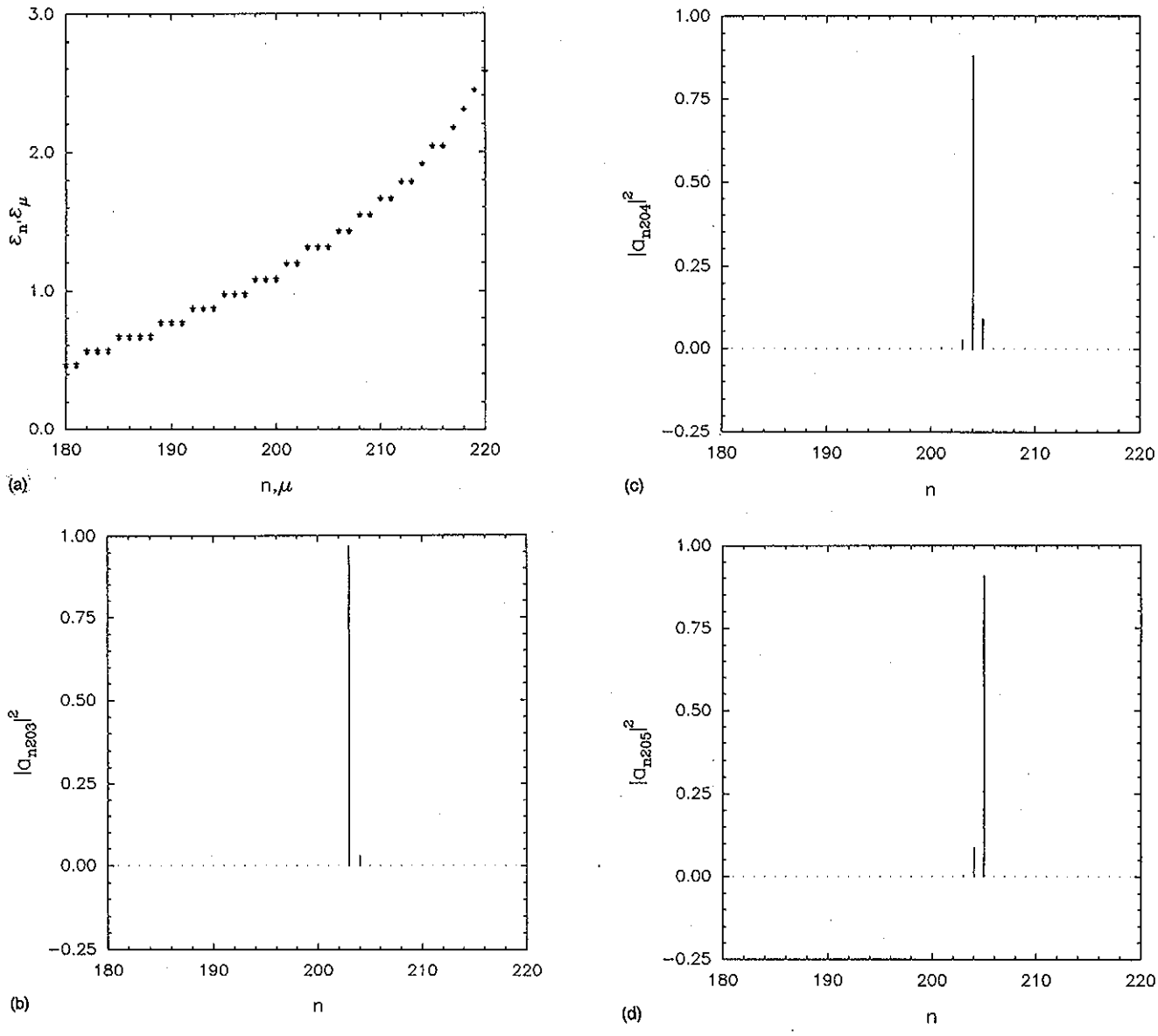

FIG. 13. (a) The same as in Fig. 11(a); (b) the same as in Fig. 11(b) for $\mu=203$; (c) the same as in (b) for $\mu=204$; (d) the same as in (b) for $\mu=205$.

was supported by CAPES (Brazil). K. F. and M. C. N. were partially supported by CNPq and FINEP (Brazil).

APPENDIX A: APPROXIMATION TO THE CLASSICAL LIMIT

The control of the approximation to the classical limit by changing the value of S, can be stated more explicitly after the observation that, in these spin systems, that limit is attained by making $S\to\infty$ and $\hbar\to 0$ with the quantity $\hbar\sqrt{S(S+1)}$ held fixed.[14,21] Therefore, by choosing the value of S, or else the energy difference between two neighboring levels, we are in fact choosing the value of the Planck constant h. Qualitative at this level, this control can be made more quantitative with the use of the data plotted in Figs. 3(a)–3(c) for the isotropic two-spin case.

Figure 3(a) shows a finite spectrum for this case, which makes valid the whole discussion on the control of the energy differences, also of the value of the Planck constant h, by changing the spin size S. The well behaved curve (a straight line) $\Delta_{n+1}\times\Delta_n$ appearing in Fig. 3(b) clearly shows a correlation between subsequent energy differences. In fact, numerical inspection of the spectrum in this case shows that

$$\Delta_{n+1}=\Delta_n+\Delta=\Delta_0+n\delta \tag{A1}$$

where Δ is constant throughout the spectrum, Δ_0 is a reference difference valid after a few first levels and δ depends only on $\hbar$ as

$$\delta=4\hbar^2. \tag{A2}$$

In this case the obtained constant δ gives $\hbar\approx 5\times 10^{-3}$, confirming the scaling relation $\hbar\sqrt{S(S+1)}=1$ for $S=200$.

Equations (A1) and (A2) can be easily inferred just by observing spectra obtained for different values of S with $\hbar$ held fixed, and comparing their energy differences with those for spectra obtained for different values of $\hbar$ with S held fixed. These relations reveal a property that can be very useful in numerical calculations where one has to simulate (semi)classical curves by what is in practice a discrete set of points. As expected, the energy difference between neighboring levels is not constant for all levels, but in these systems it increases as the upper parts of the spectra are attained [see Eq. (A1)]. Using Eq. (A2), by choosing a value for Δ sufficiently small as to prevent computational discrepancies with the classical results, one chooses in fact the Planck constant h, which can be accomplished by an appropriate value of S. This procedure can be followed for that part of the spectrum where Δ_n has its largest values: controlling this region we control the spectrum as a whole.

For the anisotropic two-spin case, however, it can be seen from Fig. 4(b) that the correlation between Δ_{n+1} and Δ_n is not so simple a relation, as Eq. (A1) is for the isotropic one. Despite the fact that in the anisotropic case this more complicated relation could still be found in principle, it is actually not necessary. For energy differences greater than 0.01—this means, for that part of the spectrum where the classical approximation would be poorer—Fig. 4(b) reproduces a straight line similar to that given by Eq. (A1). So we can follow for this case the same procedure presented after Eq. (A1). In this sense, the isotropic case can be used to calibrate this checking of the value of Planck constant necessary to a good classical approximation.

A similar analysis can be made with the data obtained for the three-spin model, for which we find

$$\Delta_{n+1}=\Delta_n+\Delta=\Delta_0+n\delta \tag{A3}$$

and, with a minor change in Eq. (A2),

$$\delta=\hbar^2. \tag{A4}$$

The constant δ obtained for the isotropic three-spin model sets $\hbar\approx 2\times 10^{-2}$, as expected from the relation $\hbar\sqrt{S(S+1)}=1$ for $S=50$.

APPENDIX B: WAVEFUNCTION ANALYSIS

In this Appendix we report the study of some eigenstates of the nearly integrable three-spin case with $\sigma=-0.05$. To give support to the procedure of selecting a spectrum out of the full (nearly) degenerate one, we have studied the projections of the anisotropic eigenstates $|\psi_\mu\rangle$ given by

$$H_3(\sigma\neq 0)|\psi_\mu\rangle=\epsilon_\mu|\psi_\mu\rangle \tag{B1}$$

onto the isotropic eigenstates $|\phi_n\rangle$ given by

$$H_3(\sigma=0)|\phi_n\rangle=\epsilon_n|\phi_n\rangle. \tag{B2}$$

Figures 11–13 show the projection coefficients

$$|a_{n\mu}|^2=|\langle\phi_n|\psi_\mu\rangle|^2 \tag{B3}$$

of the μ-states $|\psi_\mu\rangle$ versus the level index n of the isotropic spectrum ϵ_n corresponding to the states $|\phi_n\rangle$.[16] In Figs. 11(a)–13(a) we have the blown-up portions of the full spectra for $\sigma=0.0$ (points denoted by solid circles) and $\sigma=-0.05$ (points denoted by crosses), from where the μ-states $|\psi_\mu\rangle$ were chosen. From the figures we can see that

(a) as we have argued, the upper parts of the anisotropic spectra remains closer to the isotropic one, recovering the $\sigma=0$ staircase shape;

(b) the eigenstates $|\psi_\mu\rangle$ corresponding to each point of a given deformed anisotropic stair step has a dominant component in one of the isotropic steps;

(c) despite of being broken as a constant of motion, $\mathbf{T}_3^2$ shows a nearly conserved behavior in the sense that the projection of $|\psi_\mu\rangle$ concentrates on the states $|\phi_n\rangle$ of the corresponding isotropic stair step (which has a definite value for $\mathbf{T}_3^2$). This means that we still can associate the set of states $|\psi_\mu\rangle$ of a given deformed anisotropic stair step with the eigenvalue of $\mathbf{T}_3^2$ of the corresponding isotropic one. This reflects the perturbative nature of the transition isotropy → anisotropy and allows us to pick up of a given deformed stair step one representative of the values of $\mathbf{T}_3^2$.

We remark that, while the behavior described in item (a) is valid for even greater values of $|\sigma|$, the observations stated in items (b) and (c) are valid as long as we deal with small departures from the value $\sigma=0$. As we go farther away from $\sigma=0$, the projections shown in the figures exhibit sparser distributions over isotropic states $|\phi_n\rangle$ belonging to different stair steps, thus preventing us from speaking of a dominant value of $\mathbf{T}_3^2$.

[1] K. Nakamura, Y. Nakahara, and A. R. Bishop, Phys. Rev. Lett. **54**, 861 (1985); K. Nakamura and A. R. Bishop, Phys. Rev. B **33**, 1963 (1986).

[2] G. Q. Pellegrino, K. Furuya, and M. C. Nemes, Chaos, Solitons Fractals **3**, 327 (1993).

[3] H. Hirooka, Y. Yotsuya, Y. Kobayashi, and N. Saito, Phys. Lett. A **101**, 115 (1984).

[4] D. Farrelly, Phys. Lett. A **104**, 63 (1984).

[5] M. V. Berry, Phys. Lett. A **104**, 306 (1984).

[6] H. Hirooka, M. Kurokawa, and N. Saito, J. Phys. Soc. Jpn. **54**, 3209 (1985).

[7] O. Bohigas, in *Chaos and Quantum Physics* (Les Houches, Session LII), edited by M.-J. Giannoni, A. Voros, and J. Zinn-Justin (North-Holland, Amsterdam, 1991), and references therein.

[8] E. H. Lieb, Commun. Math. Phys. **31**, 327 (1973); K. Millard and H. Leff, J. Math. Phys. **12**, 1000 (1971).

[9] All the analysis presented in this paper follows analogously for the ferromagnetic case $J<0$ with a corresponding change in all energy signs.

[10] The fermionic case is studied in a completely similar manner.

[11] For semiclassical methods related to coherent state procedures used with the systems we treat, see for example: P. Leboeuf and M. Saraceno, Phys. Rev. A **41**, 4614 (1990); J. Kurchan, P. Leboeuf, and M. Saraceno, Phys. Rev. A **40**, 6800 (1989); D. C. Meredith, S. E. Koonin, and M. R. Zirnbauer, Phys. Rev. A **37**, 3499 (1988).

[12] M. Oliveira Terra (private communication).

[13] The well defined frequencies shown in Fig. 3(c) could provide, with appropriate scale factors, a simple estimate of the period of the orbits. Though rough, this estimate would allow us to avoid the numerical integration of the corresponding Hamilton equations of motion and the elliptic integrals obtained in analytical calculations (see Ref. 2).

[14] L. E. Reichl, *The Transition to Chaos in Conservative Classical Systems: Quantum Manifestations* (Springer-Verlag, New York, 1992), see especially Chap. 5 on spin systems and references therein.

[15] In using the strategy presented at the end of Sec. IV A, we try to keep the initial spirit of the paper, which means to get as much information as possible from the simple plots $\Delta_{n+1}\times\Delta_n$ and $\Delta_n\times n$, without delving into more complicated matters such as symmetries or more sophisticated tech-

niques to explore chaoticity. These points are reserved to a future work.
[16] L. Benet, T. H. Seligman, and H. A. Weidenmüller, Phys. Rev. Lett. **71**, 529 (1993).
[17] A. J. Lichtenberg and M. A. Lieberman, *Regular and Stochastic Motion*, Applied Mathematical Sciences (Springer-Verlag, New York, 1983), Vol. 38; E. Ott, Rev. Mod. Phys. **53**, 655 (1981).
[18] Y. Alhassid and R. D. Levine, Phys. Rev. A **40**, 5277 (1989); M. Feingold, in *Chaos, Noise and Fractals*, edited by E. R. Pike and L. A. Lugiato (Adam Hilger, Bristol, 1987); M. V. Berry and M. Robnik, J. Phys. A **17**, 2413 (1984).
[19] H. J. Lipkin, N. Meshkov, and A. J. Glick, Nucl. Phys. **62**, 188 (1965).
[20] M. C. Cambiaggio, G. G. Dussel, and M. Saraceno, Nucl. Phys. A **415**, 70 (1984).
[21] Setting $\hbar=1$ does not affect the discussion on the classical limit. In fact, making $S\to\infty$ and $\hbar\to 0$ with $\hbar\sqrt{S(S+1)}=1$ is equivalent to set $\hbar=1$ and scale the resulting energies by $\hbar^2 S(S+1)$, as we do throughout this paper. Both procedures give the same results but the second one makes numerical calculations easier. Also the chosen scale factor is largely a matter of convenience: here we use $J\hbar^2 S(S+1)$ taking advantage of the above discussion on the classical limit; in Ref. 2, for example, the factor JS^2 appears in the corresponding classical Hamiltonian $\mathscr{H}$, becoming the natural choice.